Supporting Information

Self-powered integrated system of strain sensor and flexible all-solid-state supercapacitor by using high performance organohydrogel electrolyte

Jianren Huang, Shuijiao Peng, Jianfeng Gu, Guoqi Chen, Jianhong Gao, Jin Zhang, Linxi Hou, Xiaoxiang Yang, Xiancai Jiang, Lunhui Guan**

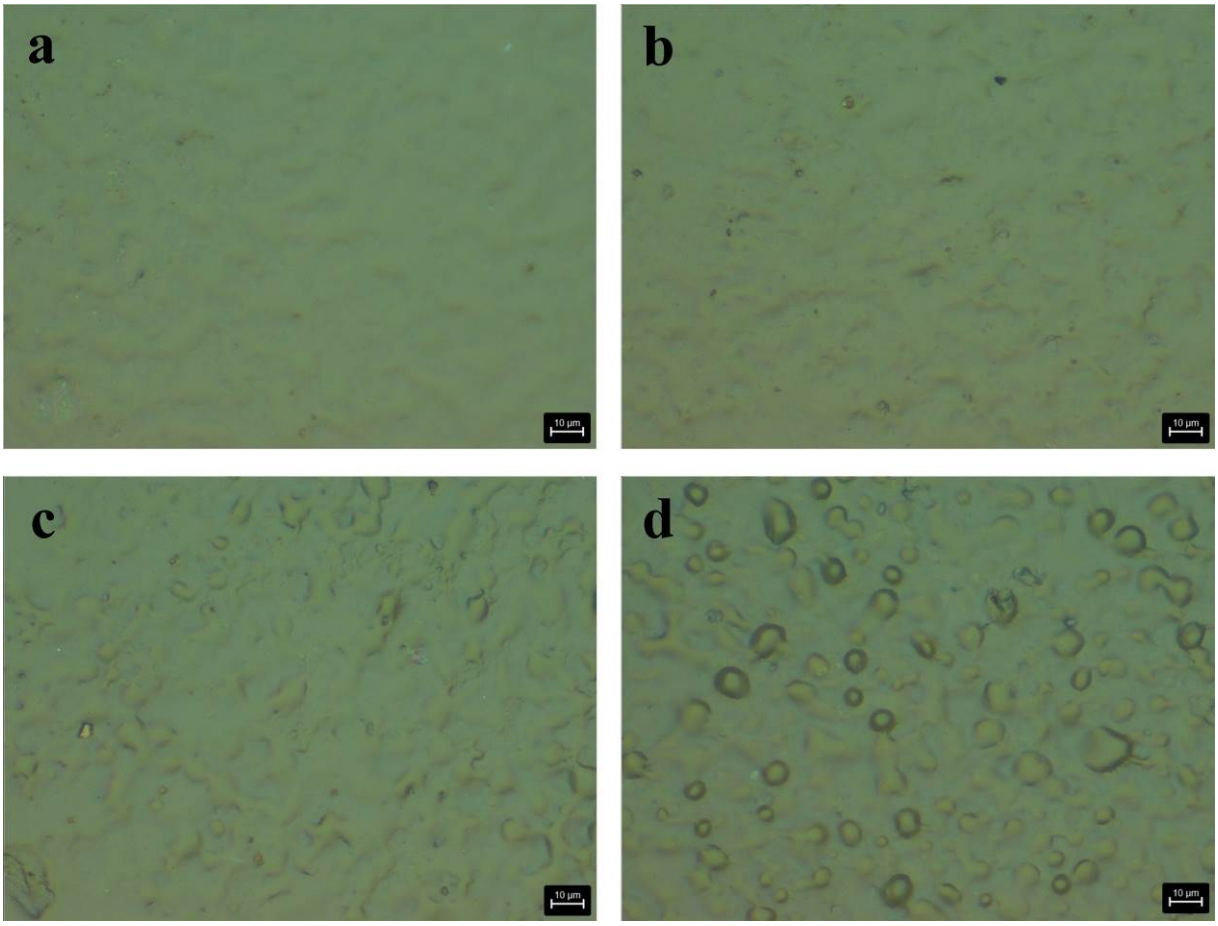

Figure S1. Optical microscope images of a) PPGN-0, b) PPGN-1, c) PPGN-2, and d) PPGN-3 ionic organohydrogels. The scale bar was 10 μm.

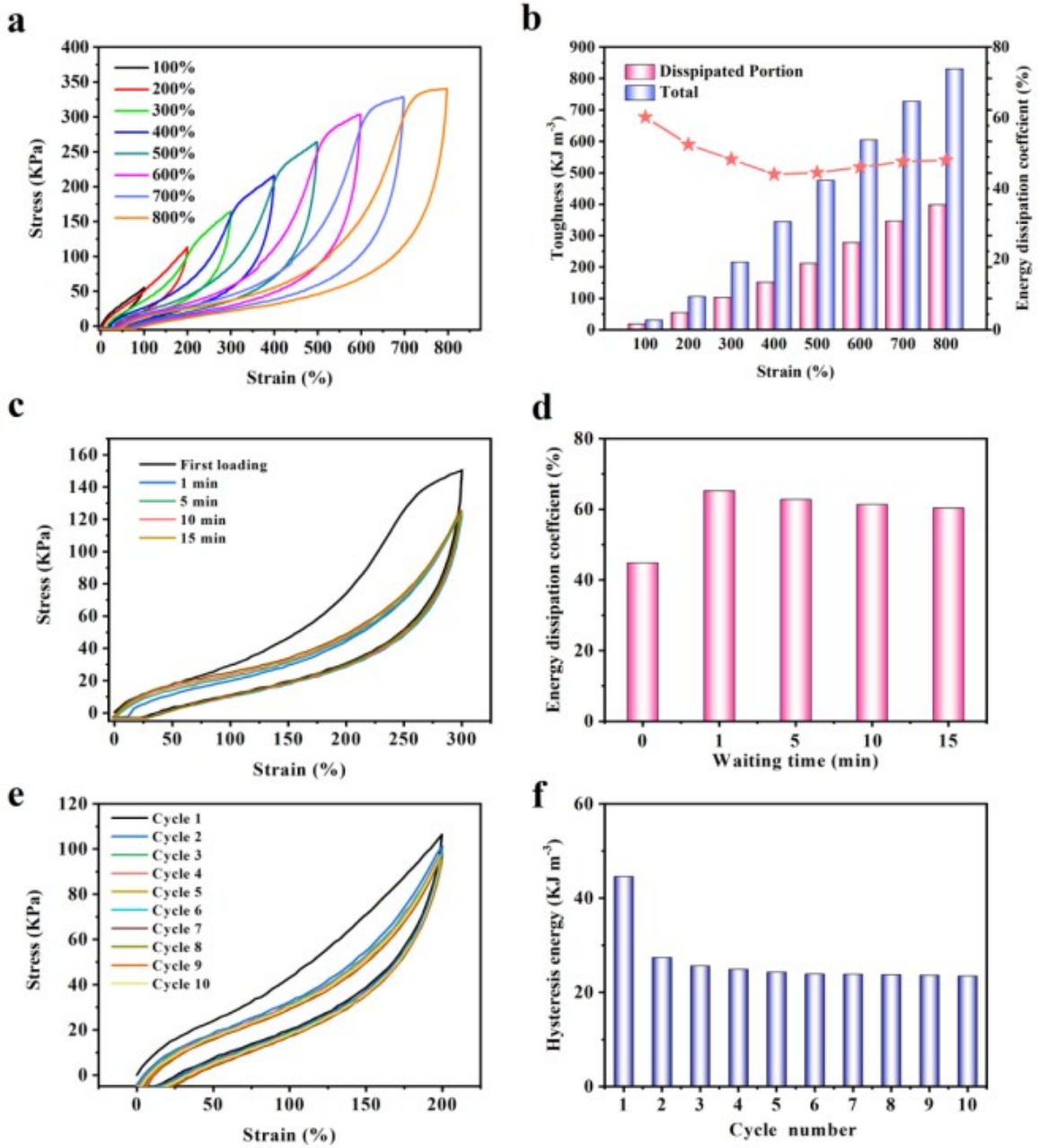

Figure S2. The strain cycling tests of the PPGN-3 organohydrogel under various conditions. (a) Loading-unloading curves and (b) corresponding toughness/energy dissipation at different maximum strain. (c) Cyclic loading-unloading curves at the maximum strain of 300% for different resting time between two consecutive tests. (d) Energy dissipation coefficient at different resting time. (e) Ten successive cyclic loading-unloading curves at tensile strain of 200% with 1 min resting time between two consecutive tests. (f) The hysteresis energy during various loading cycles.

For cyclic tensile tests, the organohydrogel specimen was stretched to a preset maximum strain and then returned to the initial length at the same deformation rate. For the recovery experiment, the organohydrogel specimen was initially stretched to a predetermined strain of 300% and then reloaded at the same rate after the sample was relaxed for predetermined time (0−15 min). Ten cycles were performed on the organohydrogel in the cyclic tensile test.

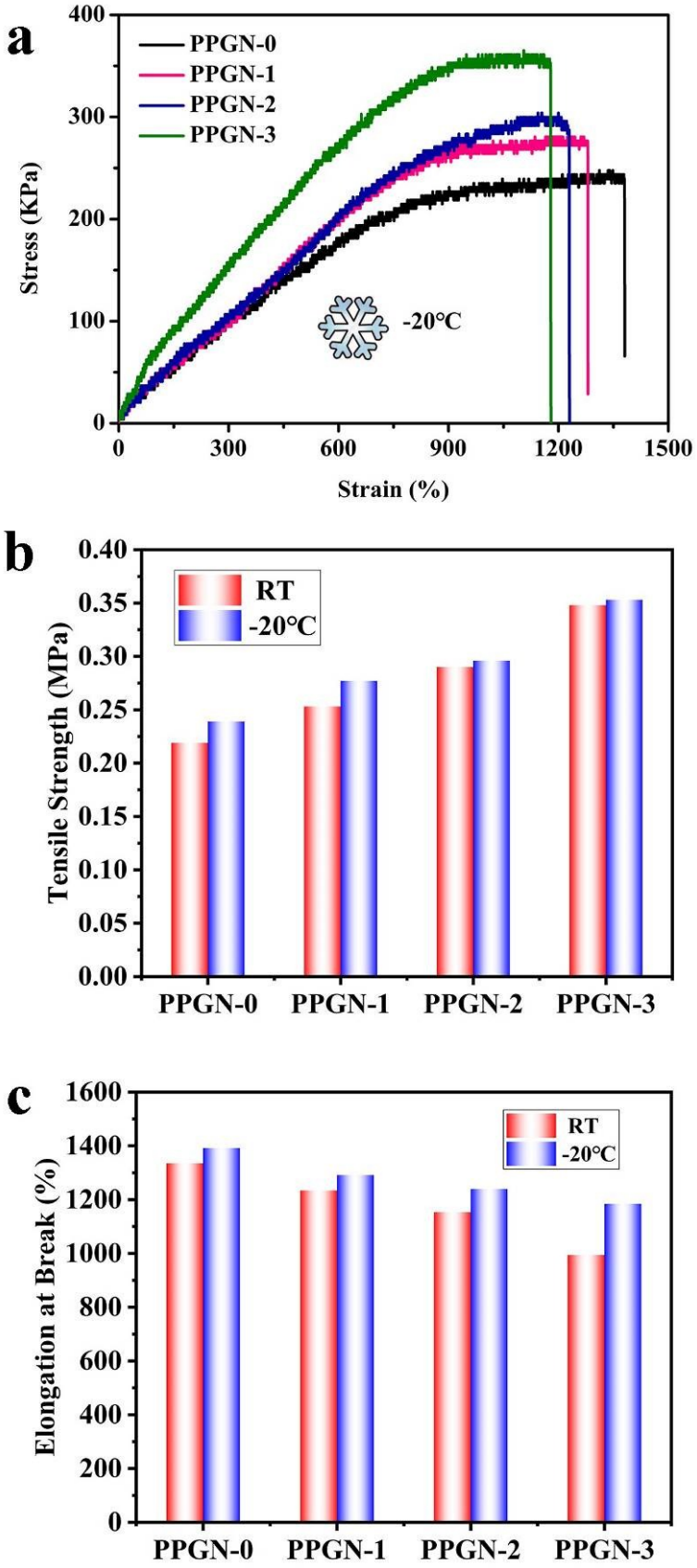

Figure S3. The mechanical properties of PPGN-0, PPGN-1, PPGN-2, and PPGN-3 ionic organohydrogels under -20 ℃: a) typical stress-strain tensile testing curves, b) tensile strength, and c) elongation at break.

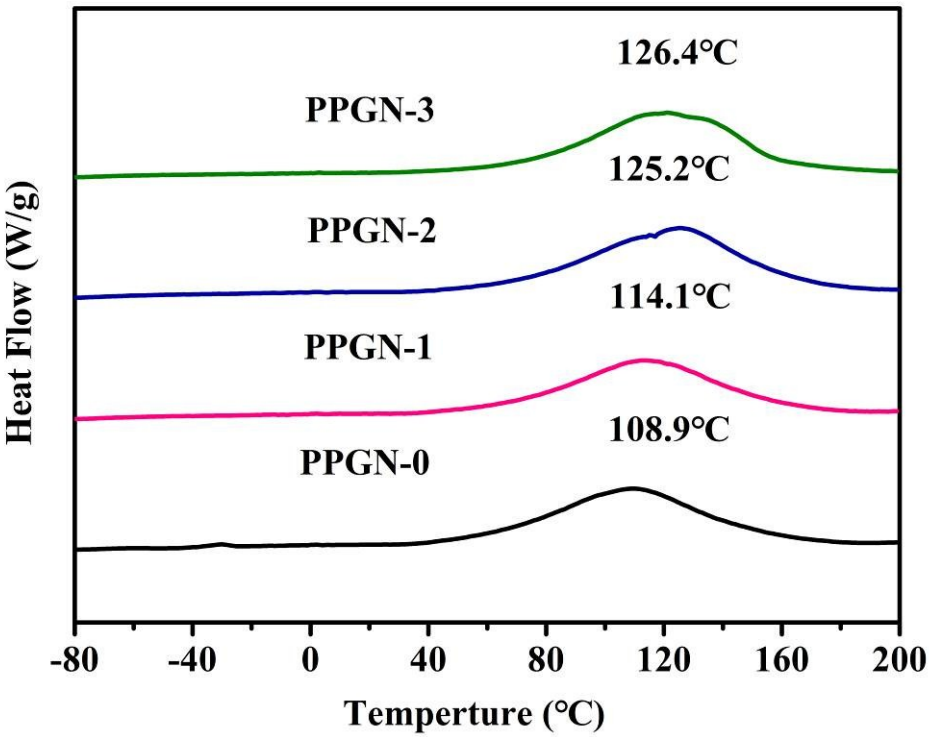

Figure S4. DSC curves of PPGN-0, PPGN-1, PPGN-2, and PPGN-3 ionic organohydrogels.

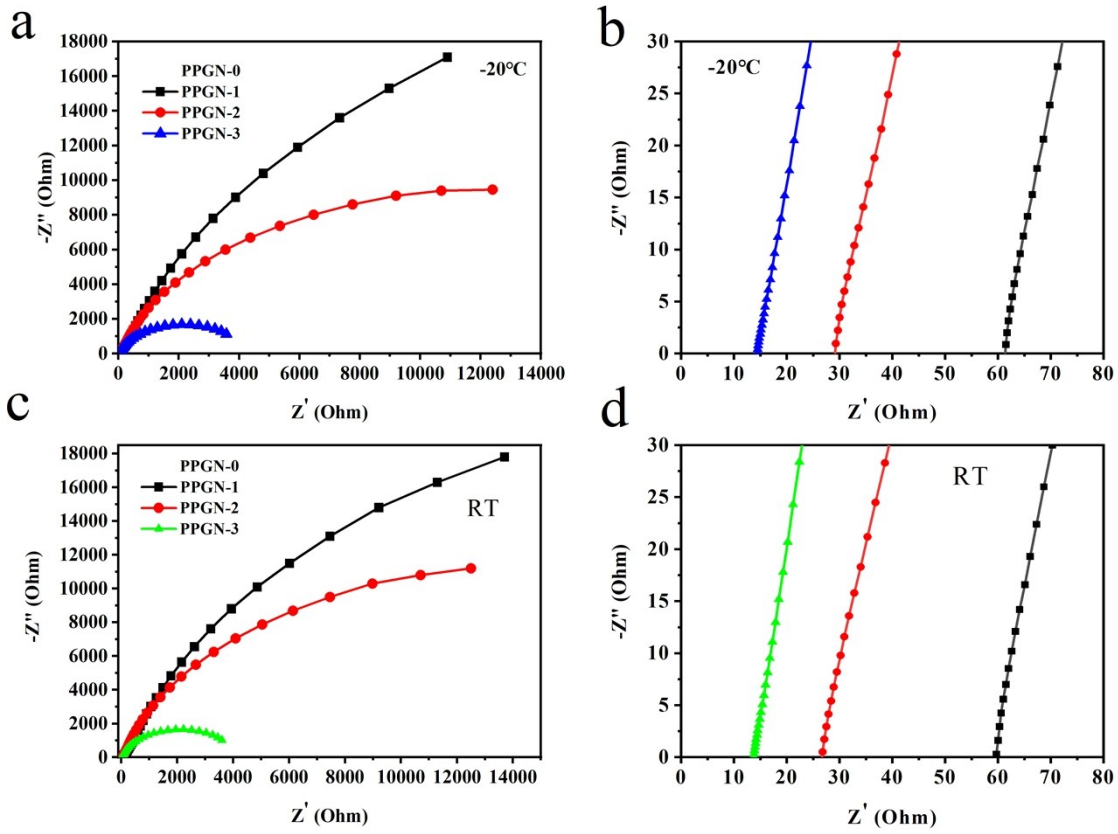

Figure S5. The EIS curves of PPGN-0, PPGN-1, PPGN-2, and PPGN-3 organohydrogel at-20 °C (a, b) and room temperature (c, d).

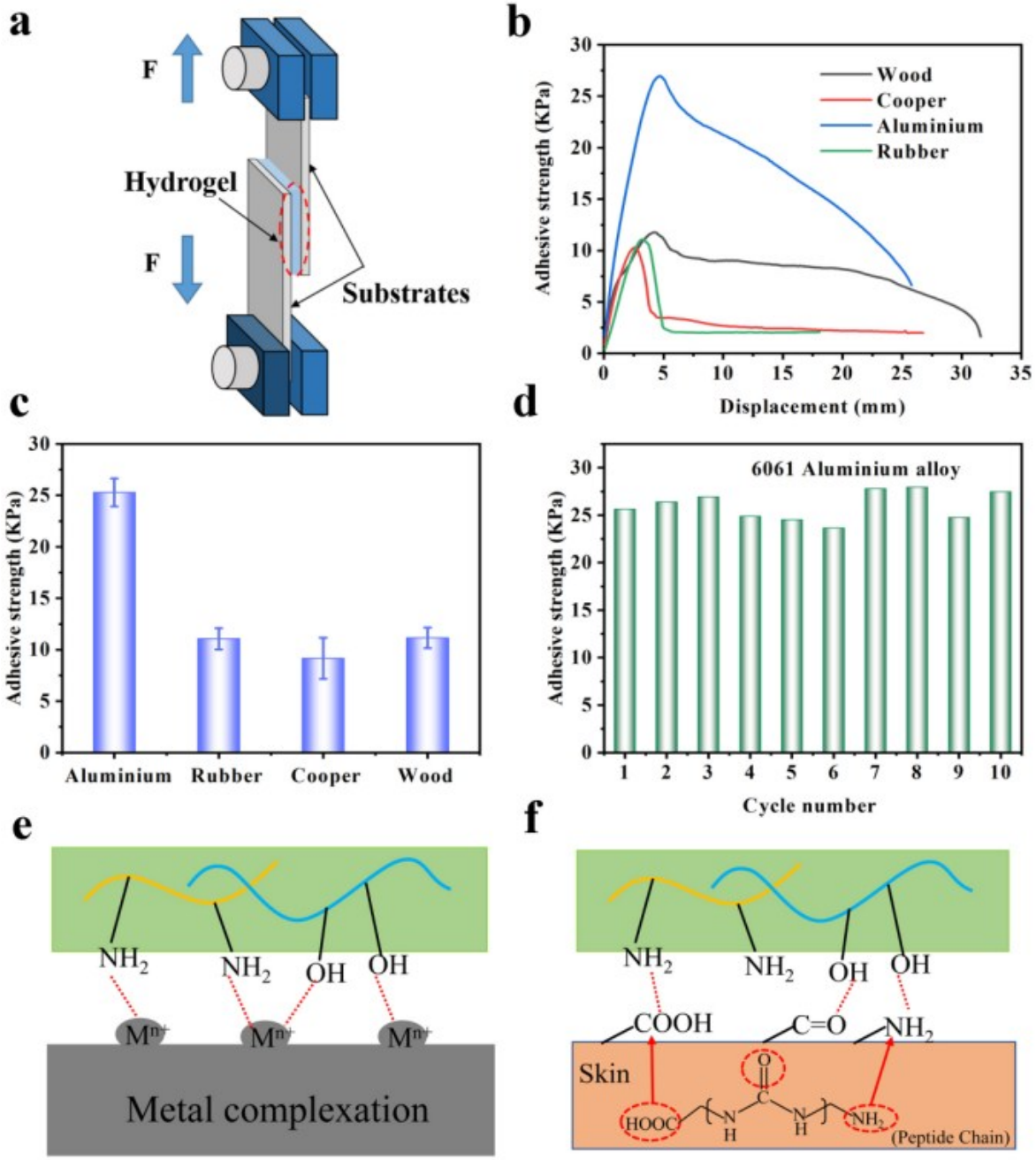

Figure S6. Adhesive properties of PPGN-3 organohydrogel (a) Schematic description of lap shear test. (b) Representative curves of adhesion shear force versus displacement for organohydrogels with different substrates (wood, copper, aluminum and rubber). (c) the corresponding adhesion strength. (d) Repeatable adhesive behaviors of the organohydrogel to 6061 aluminum alloy surface conducted by 10 continuous cyclic lap shear tests. (e) and (f) The adhesion mechanism of the PVA/PAMAA/Gly/NaCl organohydrogel.

As illustrated in Figure S6a, a hydrogel plate (25 mm×25 mm×2 mm) was placed between two substrates (i.e. hydrophilic wood, copper, rubber and aluminum) to form a sandwiched area of 15 mm×15 mm. A contact pressure (100 g) was applied for 5 min to form a good contact before the measurement. Afterward, the samples were pulled at a fixed speed of 10 mm min^{-1} until separation by a universal mechanical machine under room temperature and the adhesive strength was calculated by the maximal load divided by the initial attached area. Measurements of each assembly were repeated at least five times and the results were reported as mean ±

standard deviation. For the repeated adhesion, the waiting time attached to the surface of substrates was 10 min. The next test was conducted immediately after each test.

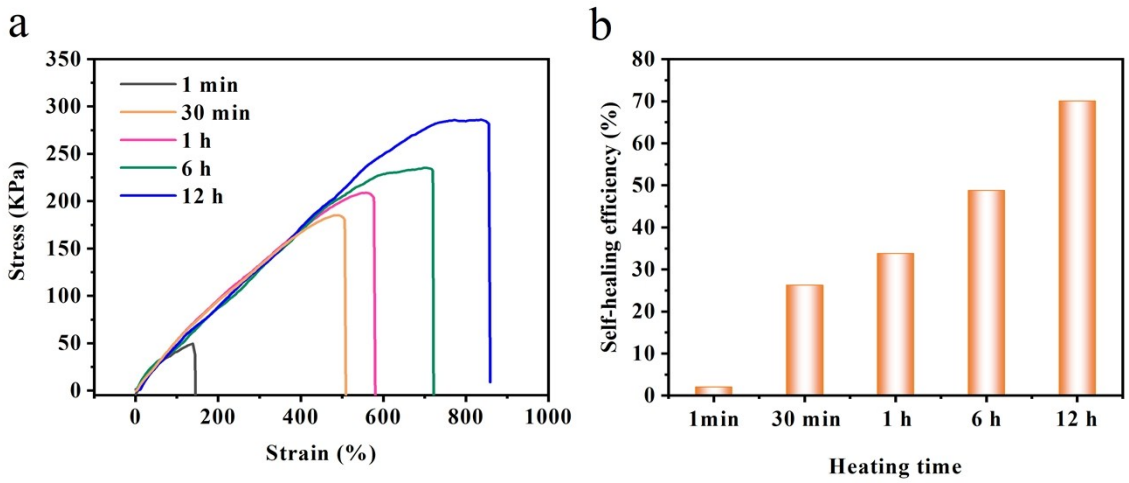

Figure S7. Self-healing properties of PPGN-3organohydrogel. (a) Tensile stress-strain curves of organohydrogel at different healing time. (b) Corresponding self-healing efficiency of toughness.

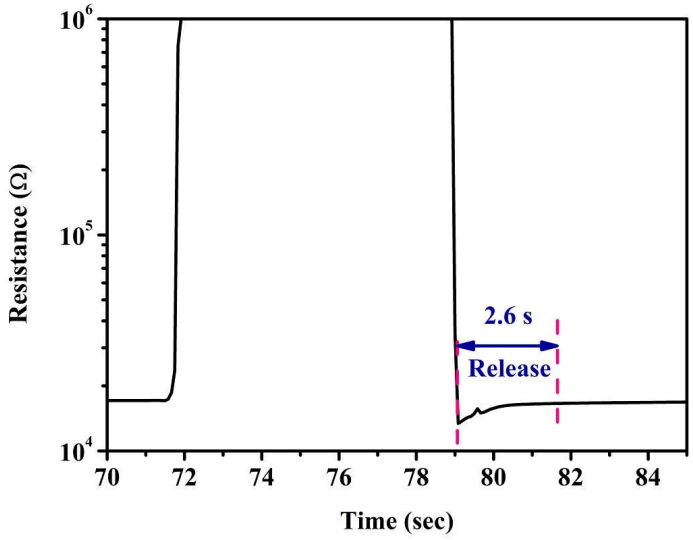

Figure S8. The time of healing process for the PPGN-3 organohydrogel electrolyte by the real-time resistance measurement.

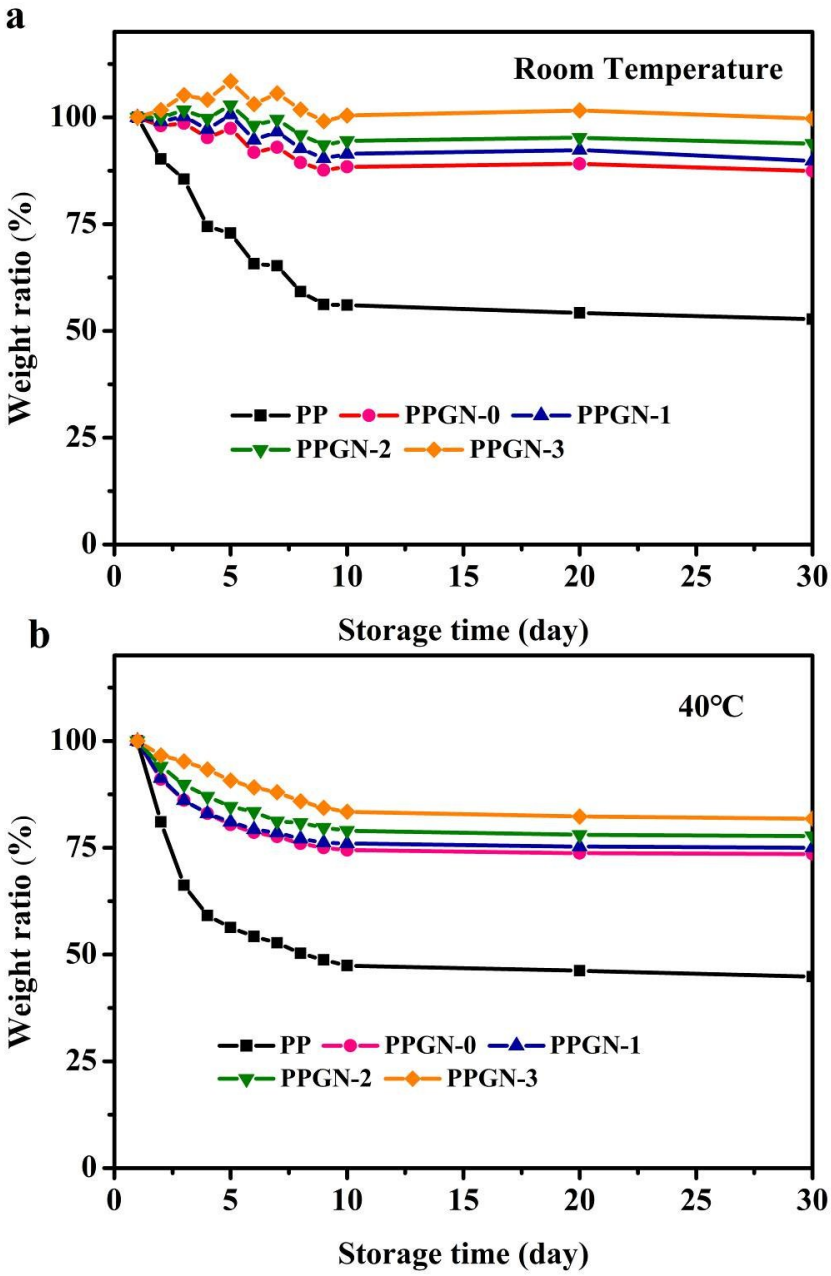

Figure S9. Weight variation ratio of ionic organohydrogel stored at a) RT and b) 40 ℃ for 30 days.

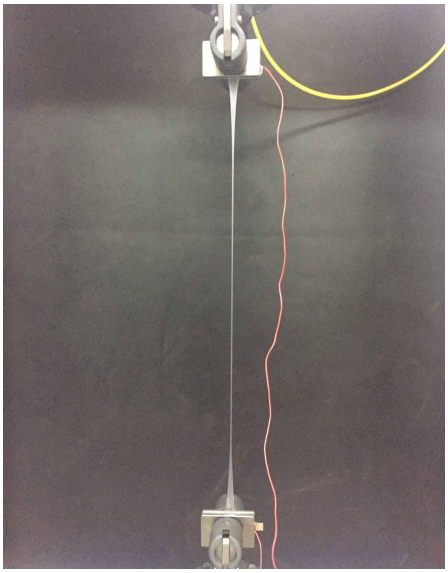

Figure S10. Digital image of the organohydrogel stretched from 0% to 1000% strain

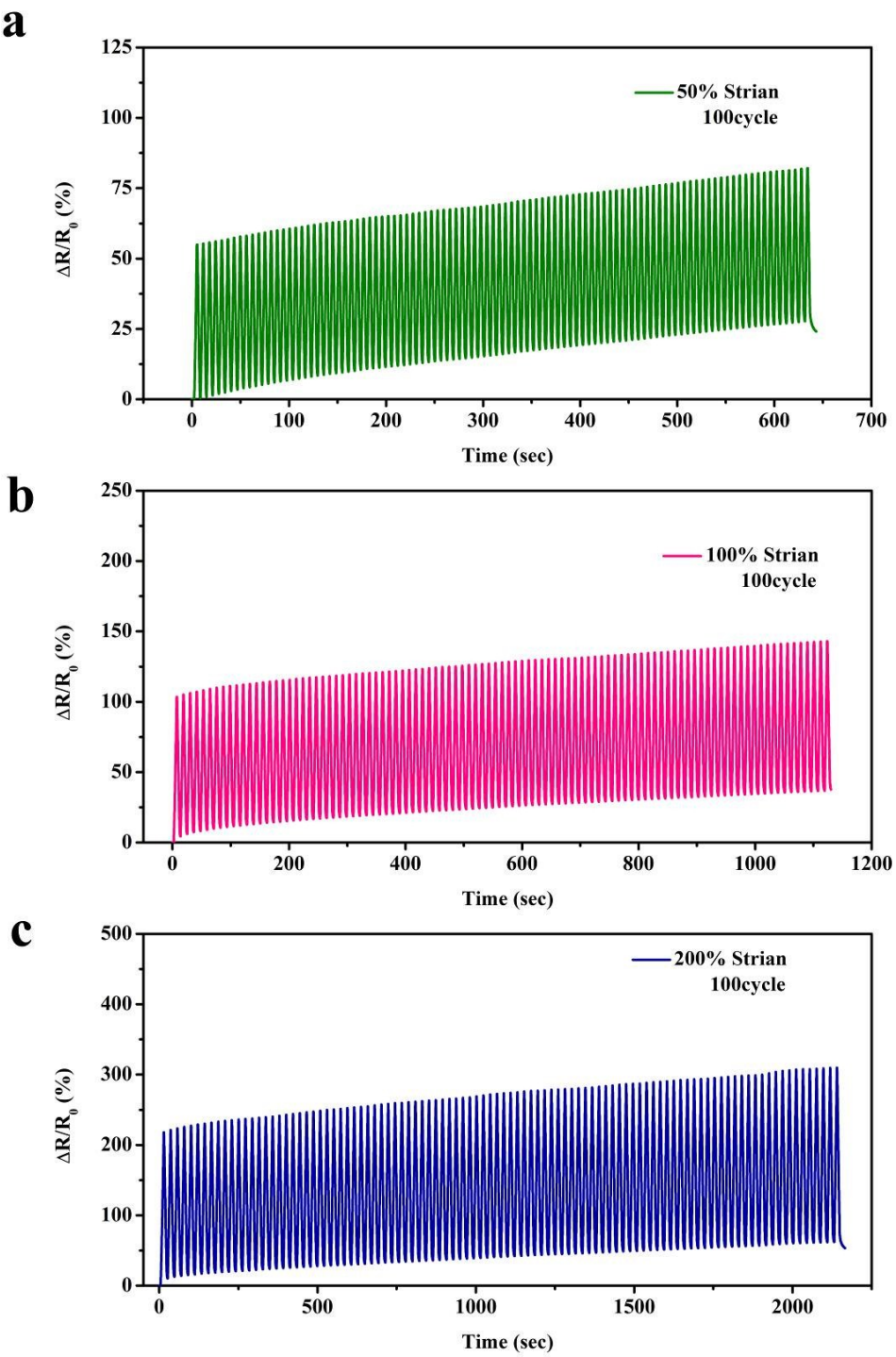

Figure S11. Resistance response of repeated stretching tests of organohydrogel strain sensor at different strains for 100 cycles: a) 50% strain, b) 100% strain, and c) 200% strain.

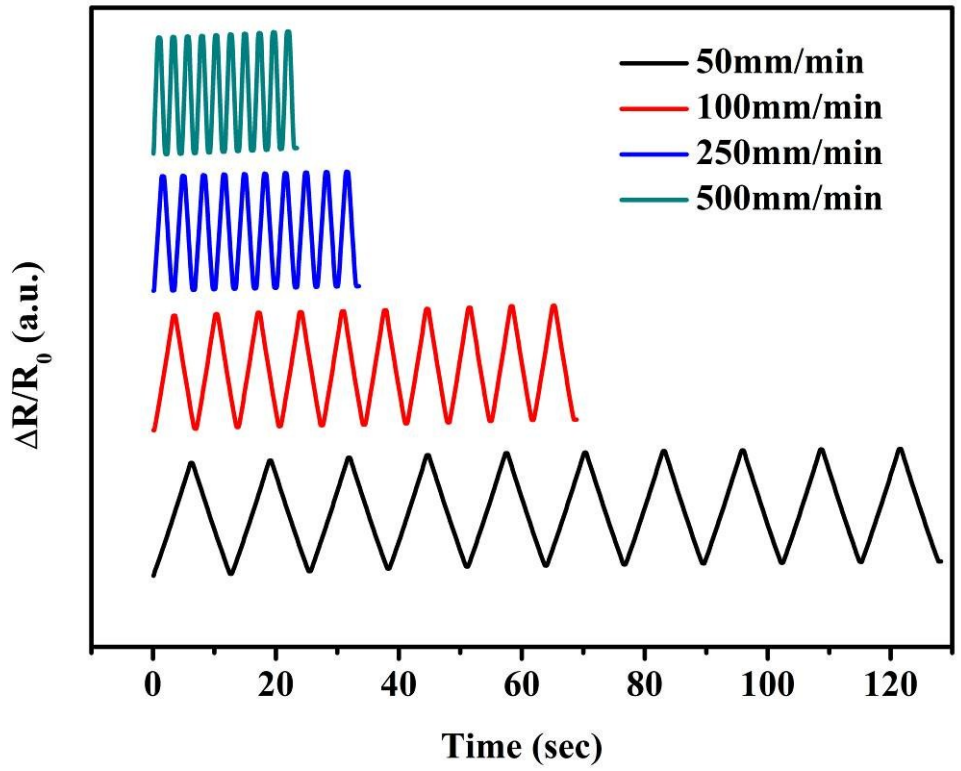

Figure S12. Resistance response of repeated stretching tests of organohydrogel strain sensor at diverse frequencies under 100% strain.

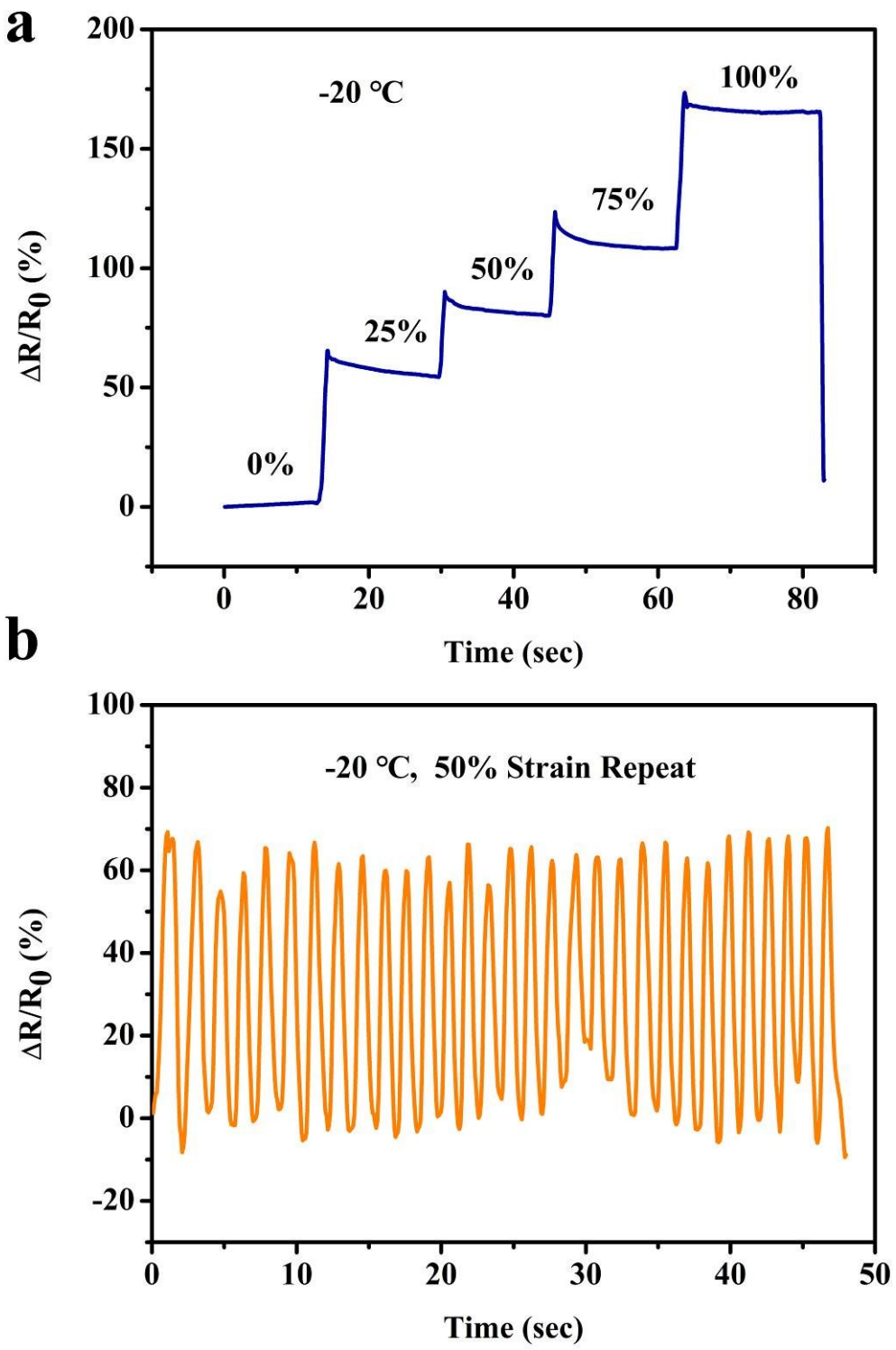

Figure S13. Electromechanical properties of the organohydrogel strain sensor at −20 °C: a) Resistance response of the hydrogel strain sensor stretched to 25%, 50%, and 100% b) Resistance responses of the sensor repeated large strains (50%).

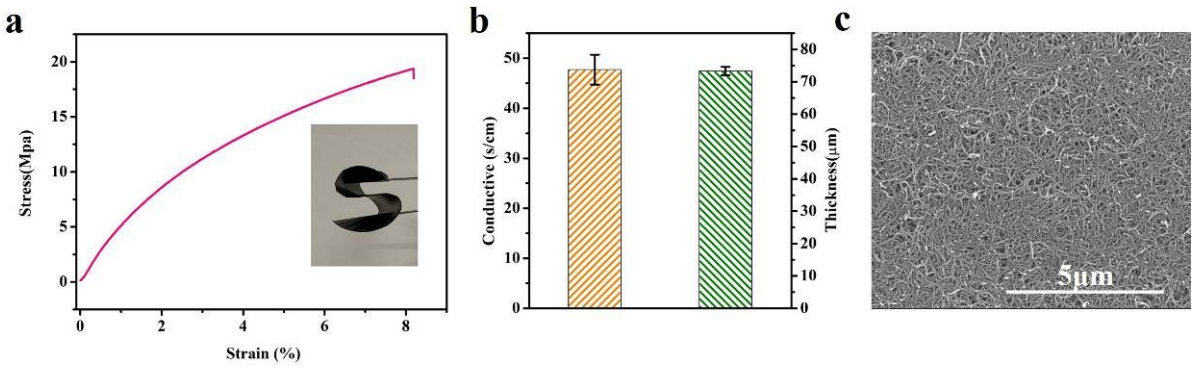

Figure S14. Characterizations of MWCNT film electrodes. a) Strain-stress curves of electrodes (inset is flexible exhibition). b) Thickness and electrical conductivity of buckpaper. c) Surface SEM image of bare MWCNT film.

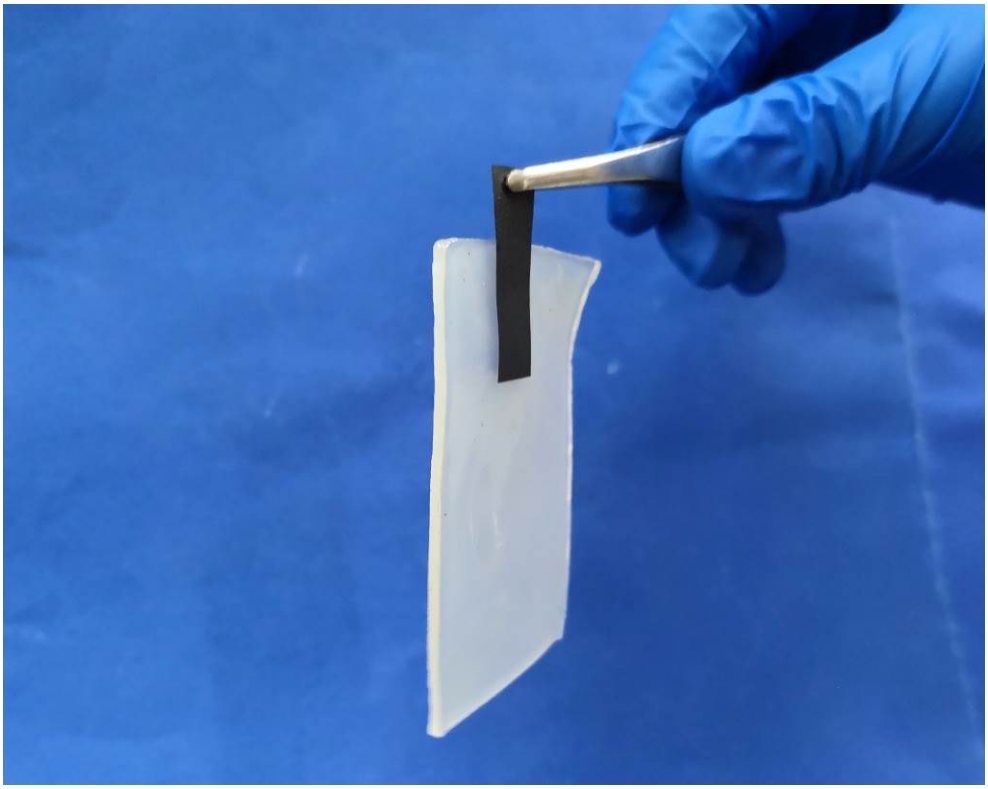

Figure S15. The photo showing good adhesion between electrode and PPGN-3 organohydrogel electrolyte due to hydrophilic interactions and hydrogen bonds.

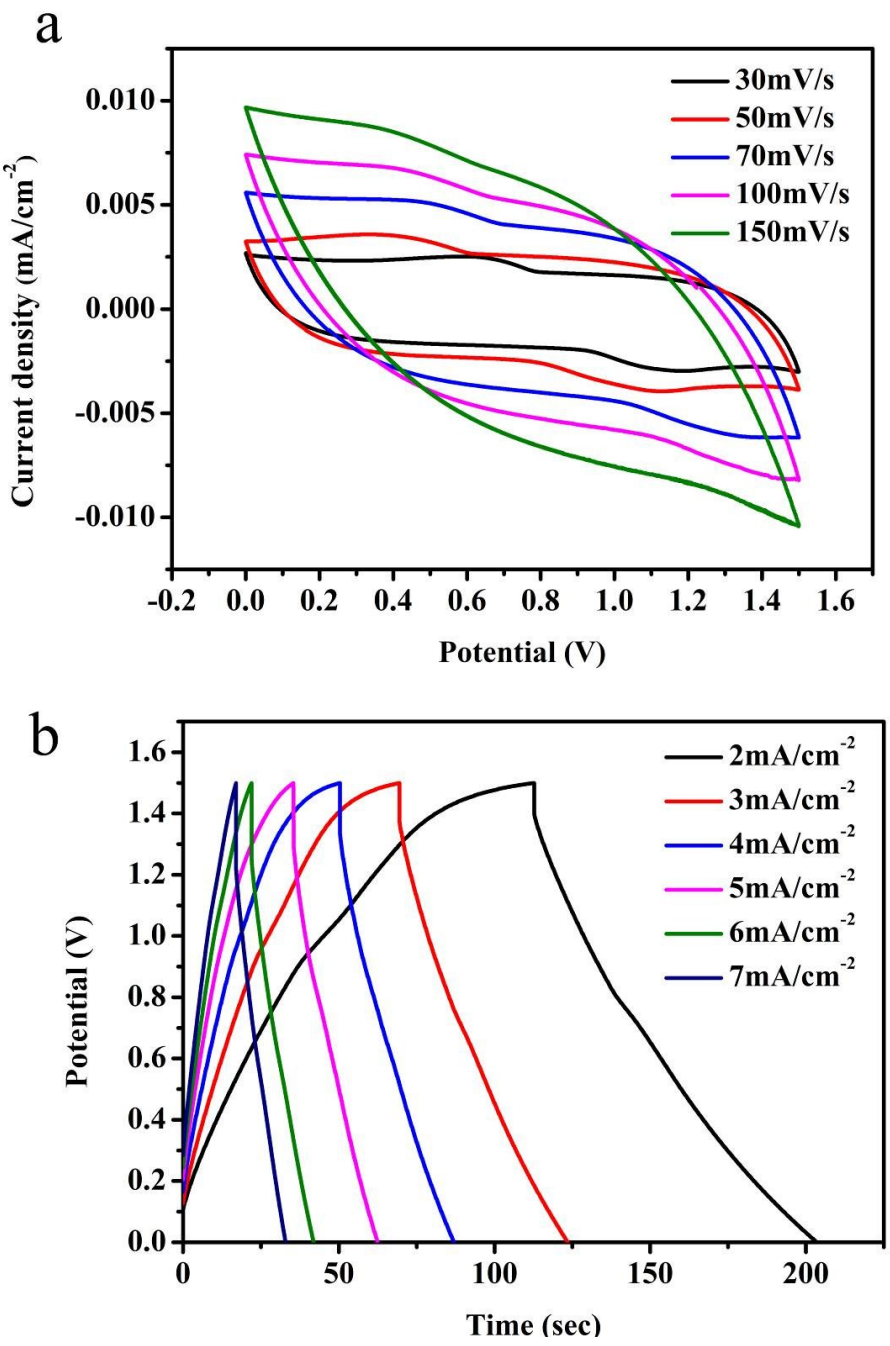

Figure S16. The CV and CGD curves of the supercapacitor at 1.5V.

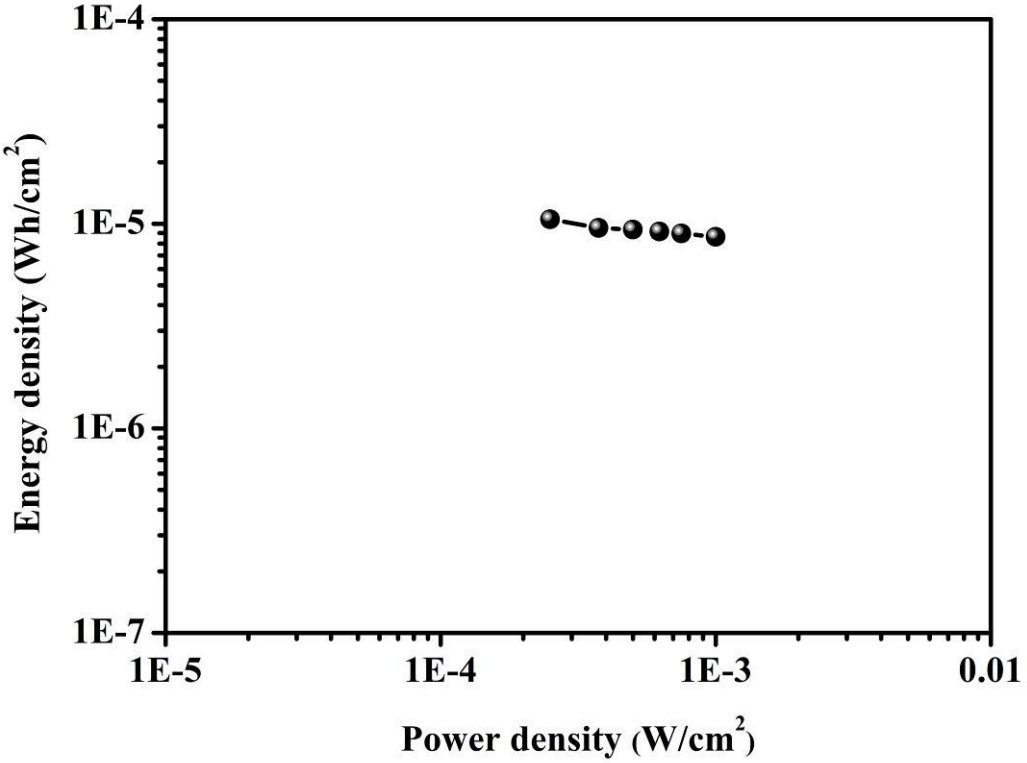

Figure S17. The energy density and power density of supercapacitor.

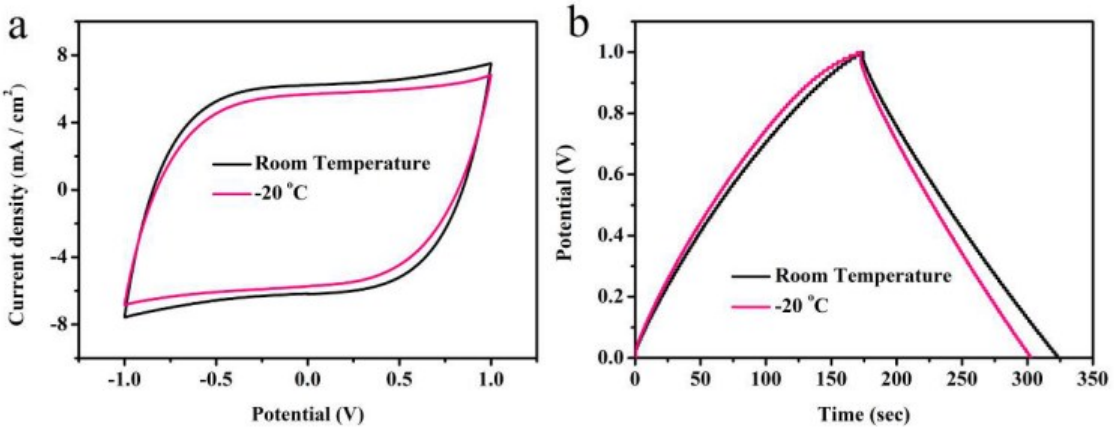

Figure S18. Comparison of all-solid-state supercapacitors based on organohydrogel electrolyte at room temperature and -20 ℃ a) CV curves at the scan rate of 100 mV s^{-1}. b) GCD curves at the current density of 0.5 mA cm^{-2}.

To evaluate the low temperature performance of organohydrogel electrolyte based supercapacitors, the prepared supercapacitor was stored at a low temperature of -20 ℃ for 24 h, and then the capacitive behaviors were researched through CV and GCD (Figure S18a, b). Although the temperature was decreased, the quasi-rectangular shape of voltammograms still can be seen. Besides, GCD measurements were carried out to characterize the cycling stability of the supercapacitor at low temperature. As shown in Figure 14c, the supercapacitor retains about 83.3% of its initial capacitance even after 5000 cycles at -20 ℃. These results proved that organohydrogel electrolyte possesses superb anti-freezing property and the supercapacitor can withstand low temperature down to -20 °C.

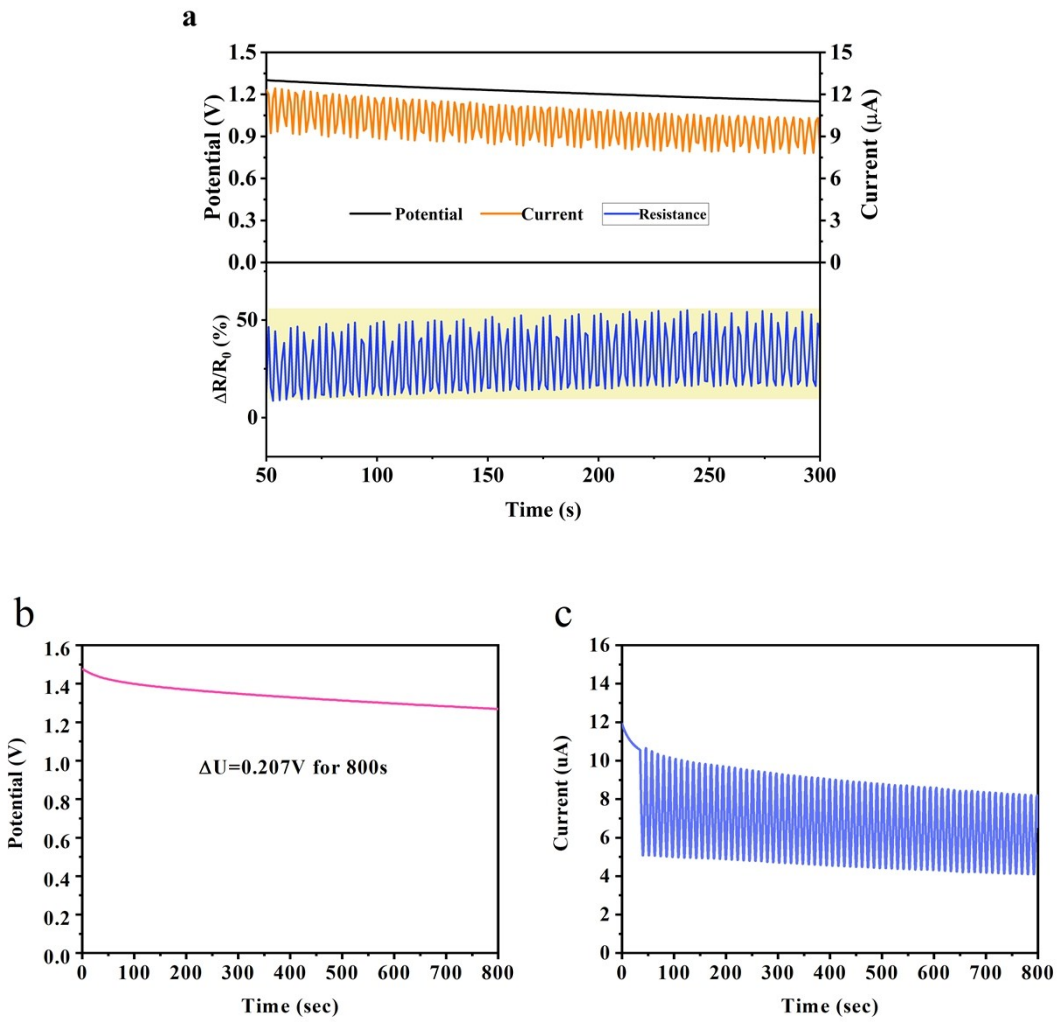

Figure S19. (a) The time electric signal response curves of strain sensor driven by supercapacitor under applied strain of 25% from 50 to 300 seconds; (b) Discharging profile of the organohydrogel supercapacitor for driving strain sensor (c) tensile strain response curves of the sensor driven by supercapacitors under applied strain of 100% for 800 seconds.

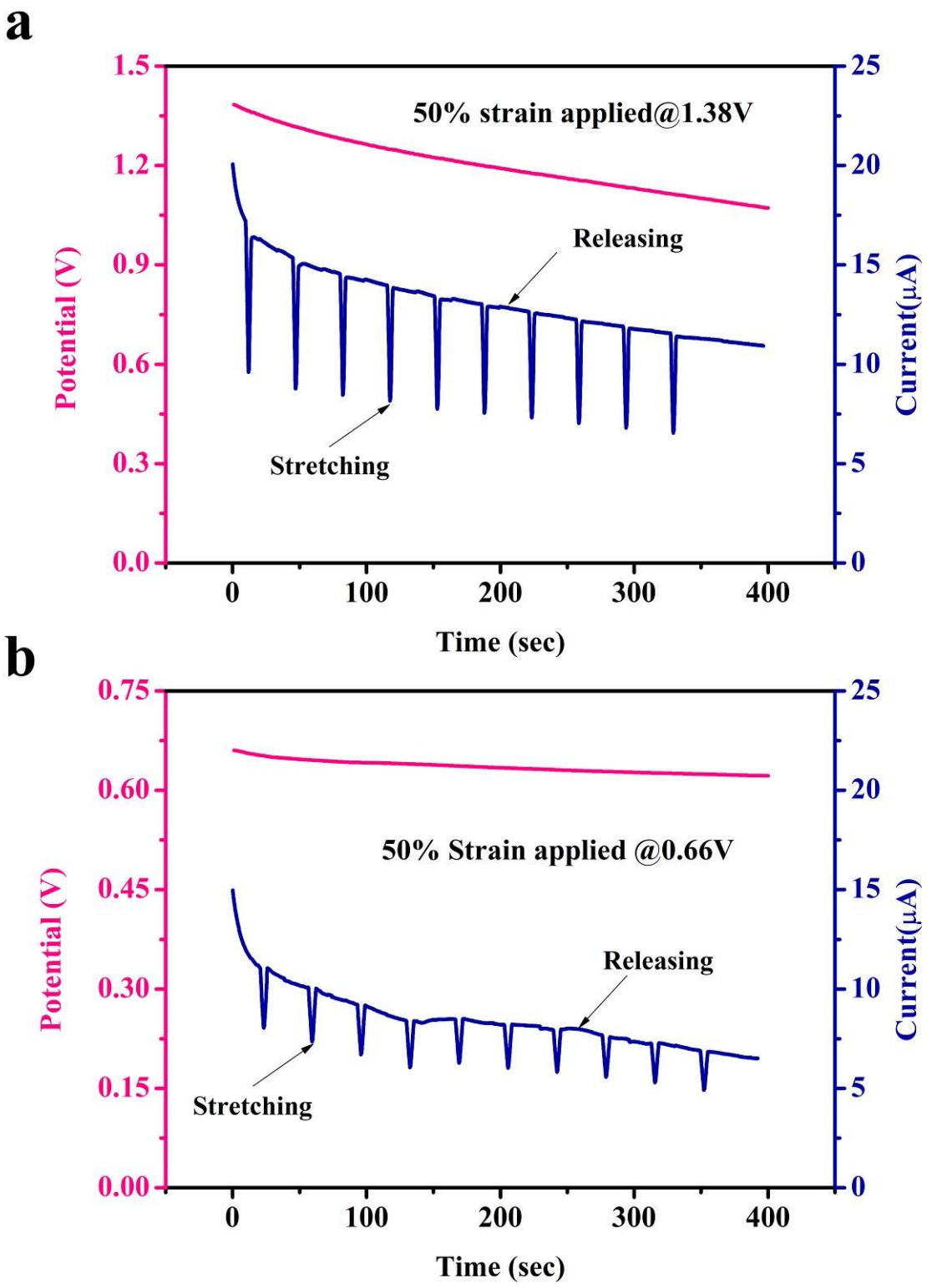

Figure S20. Change in current of strain sensor at applied voltages of 0.66 V and 1.38 V under strain of 50%.

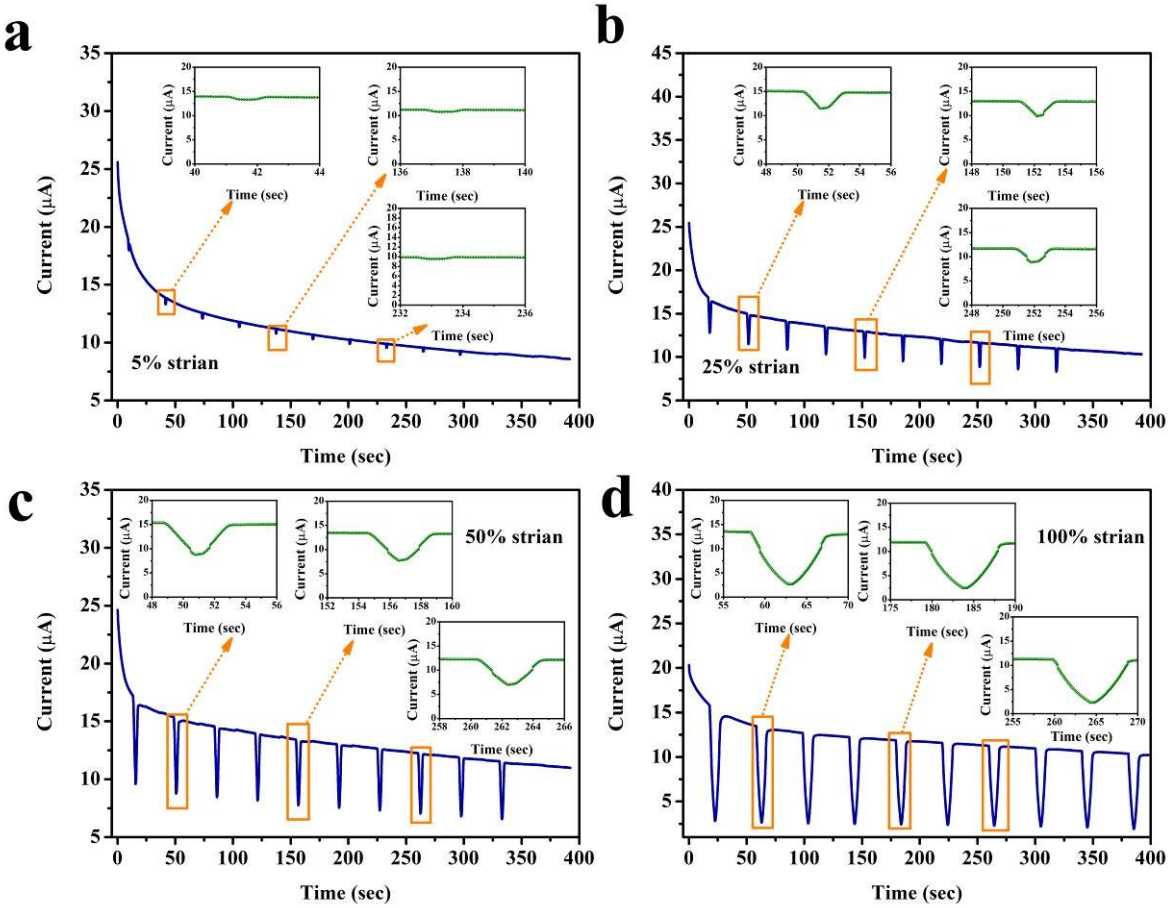

Figure S21. Strain-response curves of the strain sensor driven by flexible all-solid-state supercapacitor under strain of (a) 5%, (b) 25%, (c) 50% and (d) 100% for 10 cycles.

Figure S22. A good adhesion between organohydrogel sensor and the human skin.

Table S1 The experimental ingredients and nomenclatures of PVA/PAMAA/Gly/NaCl DN organohydrogel electrolytes.

Sample	PVA (g)	AM (g)	AA (g)	Irgacure 2959 (g)	MBA (mg)	Water (ml)	Glycerol (ml)	NaCl (g)
PPGN-0	0.2	1.9936	0.107	0.0662	1.36	4.0	3.0	0
PPGN-1	0.2	1.9936	0.107	0.0662	1.36	4.0	3.0	0.14
PPGN-2	0.2	1.9936	0.107	0.0662	1.36	4.0	3.0	0.42
PPGN-3	0.2	1.9936	0.107	0.0662	1.36	4.0	3.0	0.70

Table S2. Comparison of our work with other reported flexible hydrogel-based strain sensors

Base gel	Gauge factor (tensile)	Sensing range (%)	Response time (s)	Anti-freezing	Adhesive	Non-volatile	Self-Healing	Reference
PVA/PAMAA/Gly NaCl	***8.303***	***1000***	***0.16***	***Yes***	***Yes***	***Yes***	***Yes***	***Our work***
PAAm/LiCl	0.84	40	N/A	N/A	N/A	N/A	N/A	*Adv. Mater. 2017* [1]
PVA/SWCNT	1.51	1000	N/A	N/A	N/A	N/A	Yes	*Adv. Sci. 2017* [2]
TA@CNC/Al^{3+}	7.8	2000	N/A	N/A	Yes	N/A	Yes	*Chem. Mater. 2018* [3]
PVA/MXene	25	40	N/A	N/A	Yes	N/A	Yes	*Adv. Sci. 2018* [4]
PVA/MXene	1.2	200	0.165	N/A	N/A	N/A	Yes	*Adv. Electron. Mater 2019* [5]
PAA/Fe_3O_4	3.96	800	N/A	N/A	Yes	N/A	Yes	*Small 2019* [6]
PNIPAAm/PANI	3.92	120	0.4	N/A	N/A	N/A	N/A	*ACS Appl. Mater. Interfaces 2018* [7]
PSS/UPy/PANI	3.4	300	N/A	N/A	N/A	N/A	Yes	*Chem. Mater 2019* [8]
PDA-PAM/PANI	0.693	1000	N/A	N/A	N/A	N/A	Yes	*ACS Appl. Mater. Interfaces2018* [9]
P(AAm-co-HEMA)/PANI	1.48	300	0.2	Yes	N/A	N/A	N/A	*Chem. Mater. 2018* [10]
PAM/carrageenan/PANI	6	400	N/A	Yes	N/A	N/A	Yes	*ACS Appl. Mater. Interfaces2019* [11]
PMMA-r-PBA	2.73	850	N/A	N/A	N/A	Yes	N/A	*Adv. Funct. Mater2019* [12]
PAA/PANI/Gly	18.28	269	N/A	N/A	Yes	Yes	Yes	*ACS Nano 2019* [13]

Table S3. Compromise of our work with other reported flexible all-solid-state supercapacitors

Electrode	Electrolyte	Areal capacitance (mF cm^{-2})	Ref
CNT film	***PVA/PAMAA/Gly/NaCl***	***75.75@0.5 mA cm^{-2}***	***Our work***
CNTs film	poly(AMPS-co-DMAAm)/Laponite/GO	9 mF cm^{-2}@0.5 mA cm^{-2}	*Nat. Commun*.2019 [14]
CNT paper	PVA/Gly/LiCl	~17@0.5 mA cm^{-2}	*Adv. Energy Mater.* 2018 [15]
CNT film	PVA-H_3PO_4	61.4@1 mA cm^{-2}	*J. Mater. Chem. A* 2016 [16]
CNT film	PVA-H_3PO_4	72.9@0.5 mA cm^{-2}	*J. Mater. Chem. A 2016* [17]
PPy@CNT	PAAm/Al-alginate	~80@0.5 mA cm^{-2}	*Nano Energy* 2019 [18]
SWCNT-PANI	PVA-H_2SO_4	6.21@0.44 mA cm^{-2}	*Small* 2018 [19]
RGO film	PVA-KOH	30.94@2.5 mA cm^{-2}	*ACS Appl. Mater. Interfaces2019* [20]
PPy/GF	ACN–PC–PMMA–$LiClO_4$	89.6 @0.6 mA cm^{-2}	*Adv. Funct. Mater2018* [21]
PPy	PAAm	79.7@0.2 mA cm^{-2}	*Angew. Chemie Int. Ed 2019* [22]
RGO films	PVA-H_3PO_4	34@50 mV s^{-1}	*Adv. Mater.* 2016 [23]

Table S4. ***Comparison of self-discharge performance of the present self-power sensory system .***

Main material	Potential window	Potential attenuation	Power number	Ref
Organohydrogel	***1.47 V***	***0.207 V@800s***	***2***	***This work***
CNT-PDMS Sponge	N/A	1 V@130s	1	*Nano Energy* 2018 [24]
Graphene Foam	1.4 V	1.2 V@1000s	2	*Adv. Funct. Mater.* 2018 [21]
SPG-PDMS	1 V	1 V@ 480s	1	*Adv. Funct. Mater.*2017 [25]
$NiFe_2O_4$ fiber	1.2 V	1 V@400s	3	*Nanoscale* 2016 [26]

Supplementary References:

[1] K. Tian, J. Bae, S. E. Bakarich, C. Yang, R. D. Gately, G. M. Spinks, M. in het Panhuis, Z. Suo, J. J. Vlassak, *Adv. Mater.* **2017**, *29*, 1604827.

[2] G. Cai, J. Wang, K. Qian, J. Chen, S. Li, P. S. Lee, *Adv. Sci.* **2017**, *4,* 1600190.

[3] C. Shao, M. Wang, L. Meng, H. Chang, B. Wang, F. Xu, J. Yang, P. Wan, *Chem. Mater.* **2018**, *30*, 3110.

[4] Y. Z. Zhang, K. H. Lee, D. H. Anjum, R. Sougrat, Q. Jiang, H. Kim, H. N. Alshareef, *Sci. Adv.* **2018**, *4*, eaat0098.

[5] J. Zhang, L. Wan, Y. Gao, X. Fang, T. Lu, L. Pan, F. Xuan, *Adv. Electron. Mater.* **2019**, *1*, 1900285.

[6] L. M. Zhang, Y. He, S. Cheng, H. Sheng, K. Dai, W. J. Zheng, M. X. Wang, Z. S. Chen, Y. M. Chen, Z. Suo, *Small* **2019**, *15*, 1804651.

[7] Z. Wang, H. Zhou, W. Chen, Q. Li, B. Yan, X. Jin, A. Ma, H. Liu, W. Zhao, *ACS Appl. Mater. Interfaces* **2018**, *10*, 14045.

[8] J. Chen, Q. Peng, T. Thundat, H. Zeng, *Chem. Mater.* **2019**, *31*, 4553.

[9] X. Jing, H. Y. Mi, Y. J. Lin, E. Enriquez, X. F. Peng, L. S. Turng, *ACS Appl. Mater. Interfaces* **2018**, *10*, 20897.

[10] Z. Wang, J. Chen, Y. Cong, H. Zhang, T. Xu, L. Nie, J. Fu, *Chem. Mater.* **2018**, *30*, 8062.

[11] J. Wu, Z. Wu, X. Lu, S. Han, B. R. Yang, X. Gui, K. Tao, J. Miao, C. Liu, *ACS Appl. Mater. Interfaces* **2019**, *11*, 9405.

[12] Y. M. Kim, H. C. Moon, *Adv. Funct. Mater.* **2019**, *1*, 1907290.

[13] G. Ge, Y. Lu, X. Qu, W. Zhao, Y. Ren, W. Wang, Q. Wang, W. Huang, X. Dong, *ACS Nano* **2019**, acsnano.9b07874.

[14] H. Li, T. Lv, H. Sun, G. Qian, N. Li, Y. Yao, T. Chen, *Nat. Commun.* **2019**, *10*, 536.

[15] Q. Rong, W. Lei, J. Huang, M. Liu, *Adv. Energy Mater.* **2018**, *8*, 1801967.

[16] S. He, L. Qiu, L. Wang, J. Cao, S. Xie, Q. Gao, Z. Zhang, J. Zhang, B. Wang, H. Peng, *J. Mater. Chem. A* **2016**, *4*, 14968.

[17] H. Wang, B. Zhu, W. Jiang, Y. Yang, W. R. Leow, H. Wang, X. Chen, *Adv. Mater.* **2014**, *26*, 3638.

[18] Z. Liu, G. Liang, Y. Zhan, H. Li, Z. Wang, L. Ma, Y. Wang, X. Niu, C. Zhi, *Nano Energy* **2019**, *58*, 732.

[19] Y. Guo, K. Zheng, P. Wan, *Small* **2018**, *14*, 1704497.

[20] L. Gao, Y. Wang, X. Hu, W. Zhou, K. Cao, Y. Wang, W. Wang, Y. Lu, *ACS Appl. Mater. Interfaces* **2019**, *11*, 26288.

[21] H. Park, J. W. Kim, S. Y. Hong, G. Lee, D. S. Kim, J. hyun Oh, S. W. Jin, Y. R. Jeong, S. Y. Oh, J. Y. Yun, J. S. Ha, *Adv. Funct. Mater.* **2018**, *28*, 1707013.

[22] Y. Wang, F. Chen, Z. Liu, Z. Tang, Q. Yang, Y. Zhao, S. Du, Q. Chen, C. Zhi, *Angew. Chemie Int. Ed.* **2019**, *58*, 15707.

[23] Y. Shao, M. F. El-Kady, C. W. Lin, G. Zhu, K. L. Marsh, J. Y. Hwang, Q. Zhang, Y. Li, H. Wang, R. B. Kaner, *Adv. Mater.* **2016**, *28*, 6719.

[24] Y. Song, H. Chen, X. Chen, H. Wu, H. Guo, X. Cheng, B. Meng and H. Zhang, *Nano Energy*, 2018, **53**, 189–197.

[25] W. Li, X. Xu, C. Liu, M. C. Tekell, J. Ning, J. Guo, J. Zhang and D. Fan, *Adv. Funct. Mater.*, 2017, **27**, 1–12.

[26] L. Li, Z. Lou, W. Han and G. Shen, *Nanoscale*, 2016, **8**, 14986–14991.